Water Research 161 (2019) 549–559

Contents lists available at ScienceDirect

Water Research

journal homepage: www.elsevier.com/locate/watres

Removal of alachlor in water by non-thermal plasma: Reactive species and pathways in batch and continuous process

Niels Wardenier [a, b, *], Yury Gorbanev [c], Ineke Van Moer [b], Anton Nikiforov [a], Stijn W.H. Van Hulle [b], Pieter Surmont [d], Frederic Lynen [d], Christophe Leys [a], Annemie Bogaerts [c], Patrick Vanraes [c]

[a] Department of Applied Physics, Ghent University, Sint-Pietersnieuwstraat 41 B4, 9000, Ghent, Belgium
[b] Department of Green Chemistry and Technology, Ghent University Campus Kortrijk, Graaf Karel de Goedelaan 5, 8500, Kortrijk, Belgium
[c] PLASMANT, Department of Chemistry, University of Antwerp, Campus Drie Eiken, Universiteitsplein 1, 2610, Wilrijk, Antwerp, Belgium
[d] Separation Science Group, Department of Organic Chemistry, Ghent University, Krijgslaan 281 S4-bis, 9000, Gent, Belgium

ARTICLE INFO

Article history:
Received 23 February 2019
Received in revised form
6 June 2019
Accepted 10 June 2019
Available online 10 June 2019

Keywords:
Non-thermal plasma
Pesticides
Alachlor
Oxidative species
By-products

ABSTRACT

Pesticides are emerging contaminants frequently detected in the aquatic environment. In this work, a novel approach combining activated carbon adsorption, oxygen plasma treatment and ozonation was studied for the removal of the persistent chlorinated pesticide alachlor. A comparison was made between the removal efficiency and energy consumption for two different reactor operation modes: batch-recirculation and single-pass mode. The kinetics study revealed that the insufficient removal of alachlor by adsorption was significantly improved in terms of degradation efficiency and energy consumption when combined with the plasma treatment. The best efficiency (ca. 80% removal with an energy cost of 19.4 kWh m^{-3}) was found for the single-pass operational mode of the reactor. In the batch-recirculating process, a complete elimination of alachlor by plasma treatment was observed after 30 min of treatment. Analysis of the reactive species induced by plasma in aqueous solutions showed that the decomposition of alachlor mainly occurred through a radical oxidation mechanism, with a minor contribution of long-living oxidants (O_3, H_2O_2). Investigation of the alachlor oxidation pathways revealed six different oxidation mechanisms, including the loss of aromaticity which was never before reported for plasma-assisted degradation of aromatic pesticides. It was revealed that the removal rate and energy cost could be further improved with more than 50% by additional O_3 gas bubbling in the solution reservoir.

1. Introduction

The strong global population growth, combined with raising living standards in the last century, has forced industries to the large scale production of pharmaceuticals, organic pesticides, plasticizers, and other synthetic materials. Since 1970, these anthropogenic substances have been increasingly detected in the aquatic environment (Eggen et al., 2014). Among the different types of organic contaminants encountered in the environment, pesticides occupy a unique position, since they are mostly deliberately distributed.

Pesticides are chemical compounds that have been mainly designed to protect crops against fungal or animal pests. Indeed, their presence in the environment has been primary traced back to agricultural applications. They are divided in several groups such as carbamates, pyrethroids, neonicotinoids, organochlorine, organophosphate and biopesticides (Marican & Durán-lara, 2018). For their transfer to water bodies, several potential pathways need to be considered (Köck-Schulmeyer et al., 2013). Monitoring data have shown that pesticides are usually released into the environment by diffusive sources. One of them includes the release into the surface water, through surface runoff from agricultural fields after rainfall events. Next to that, part of the pesticide load can be mobilized through the soil, eventually ending up in the ground water. Secondary effluent originating from municipal and industrial wastewater treatment plants is considered to be the major point source

* Corresponding author. Department of Applied Physics, Ghent University, Sint-Pietersnieuwstraat 41 B4, 9000, Ghent. Belgium.
E-mail address: niels.wardenier@ugent.be (N. Wardenier).

https://doi.org/10.1016/j.watres.2019.06.022
0043-1354/

of pesticides, entering into the surface water (Luo et al., 2014).

Given the high toxicity of most pesticides, along with their persistency towards conventional biological water treatment, activated carbon adsorption and chemical oxidation are currently considered as key technologies for the remediation of pesticide containing wastewaters (Ikehata & El-din, 2005; Luo et al., 2014). Although ozonation has proved to be effective in the removal of many organic pollutants, it was shown that the vast majority of the pesticides cannot be fully removed with ozonation alone (Ikehata & El-din, 2005). It should be stressed that in deionized water, the highly selective nature of O_3, only allows for a fast reaction with a limited set of organic compounds. Many important classes of crop protection chemicals such as the organochlorine pesticides, contain multiple hetero-atoms (e.g. N,P,Cl) in their molecular structure, and are thus stabilized against direct O_3 attack. In the case of organochlorine pesticides, the values for the second-order rate constants with O_3 are usually below 20 M^{-1} s^{-1} (Von Gunten, 2003; Wols and Hofman-Caris, 2012). Furthermore, the combination of multiple oxidants generally leads to a faster decomposition of target pollutants as compared to ozonation (Oturan and Aaron, 2014). A promising alternative for the abatement of recalcitrant pesticides involves the application of non-thermal plasmas: electrical discharges sustained at atmospheric pressure and near-ambient temperature. Plasmas created in liquids or gas-liquid environments produce various oxidising reactive species ($HO^{\bullet}$, $HO_2^{\bullet}$,O, O_3, H_2O_2) which contribute to the removal of organic compounds from water (Bradu et al., 2017; Jiang et al., 2014; Tarabová et al., 2018). In plasma reactors where the discharge is initiated in the gas phase, such as the dielectric barrier discharge (DBD) reactor, mass transfer is limited by the contact time of the solution under treatment in the plasma zone. Therefore, the removal efficiency (and implicitly its energy consumption) is kinetically-controlled by the diffusion rate of plasma-generated oxidants in the liquid film (Magureanu et al., 2016). Better removal efficiencies and higher energy yields are usually achieved in reactor systems that combine plasma treatment with catalysts, such as activated carbon (Qu et al., 2009). In particular, the improved performance of these so-called plasma catalytic reactors is attributed to (i) the increased the residence time of the target compound and dissolved chemical components (i.e. H_2O_2 and O_3) on the catalyst surface, compared to the bulk liquid phase, due to adsorption and ii) the generation of reactive oxygen species (ROS), which facilitates pollutant oxidation.

Previously, we have reported the use of plasma-assisted removal of alachlor in a DBD reactor combining plasma treatment with activated carbon adsorption (Vanraes et al., 2018). In the present work, the removal and energy efficiency of (i) adsorption, (ii) adsorption coupled with plasma treatment and (iii) adsorption with plasma treatment and additional ozonation with plasma gas produced in the discharge are compared. Alachlor (ALA), a chlorinated herbicide belonging to the chloroacetanilide family, was chosen as the target pesticide. Although banned within the European Union, it is still largely detected in some parts of the world (Badriyha et al., 2003). In addition, ALA is well-studied in terms of removal by different advanced oxidation processes, making it a fitting model compound.

Because the remediation of pesticide-containing wastewaters can either be carried out in reactors operated in a batch or single-pass (flow-through) configuration, the performance of both reactor modes was compared in this study, in terms of removal efficiency and energy costs. The production of various chemical oxidants (plasma-induced reactive species) was studied to obtain a better understanding of the underpinning mechanisms that contribute to ALA elimination. Finally, oxidation by-products formed during the oxidation of the pesticide were identified, and the degradation pathways were suggested.

2. Materials & methods

2.1. Chemicals

Dry oxygen (>99.5%) used as the feed gas in the plasma experiments was supplied by Air Liquide® (Belgium). Alachlor (ALA, 98%), 4-oxo-2,2,6,6-tetramethyl-1-piperidine (4-oxo-TEMP, 98%), sulphuric acid (H_2SO_4, 96%) and Titanium(IV)oxysulfate ($TiOSO_4$, 98%) were obtained from Sigma Aldrich® (Belgium). Sodium azide (NaN_3, 99%), hydrogen peroxide (H_2O_2, 30 v/v %), and dichloromethane (CH_2Cl_2, 99%) were purchased from Carl Roth® (Belgium). All chemicals and solvents were used as received.

2.2. Solution preparation

A saturated ALA solution was prepared by dissolving 50 mg of ALA powder in 100 mL of deionized water. The solution was stirred for 3 h, filtrated and finally diluted with deionized water to obtain a working solution with 1 mg L^{-1} ALA solution, which was used in the experiments. It should be noted that the ALA concentration of 1 mg. L^{-1} used in this work is higher than expected for real contaminated water conditions. Higher initial pollutant concentration usually results in the competition of the target compound with the by-products and the wastewater constituents (i.e. dissolved organic compounds) for the reaction with the oxidative species, as explained in Wardenier et al. (2019). Therefore, for real wastewater treatment the application efficiency of the process studied here may be higher than the energy costs reported in section 3.

2.3. Experimental setup

Both the batch-recirculation and single-pass experiments were carried out in the plasma-ozonation reactor (Fig. 1). The detailed setup description is found elsewhere (Vanraes et al., 2018; Wardenier et al., 2019). The reactor system consisted of a solution reservoir, connected in series with a dielectric barrier discharge (DBD) plasma reactor with cylindrical geometry. The plasma reactor consisted of a stainless steel tube, covered by one layer of Zorflex® activated carbon textile with 0.5 mm thickness, and was mounted in the centre of a quartz glass vessel. A copper mesh wrapped around the quartz vessel served as high voltage (HV) electrode. Dry oxygen was supplied at the bottom of the plasma chamber, which served as plasma feed gas. In all experiments, the gas flow rate was fixed at 1 standard liter per minute (slm) using a Bronckhorst® mass flow controller, giving a gas residence time of 1.98 s in the discharge zone. The length of the discharge region was 150 mm with a discharge gap of 2.25 mm and discharge volume of 33.1 cm^3.

The high voltage electrode was connected to an alternating-current (AC) power supply, generating sinusoidal voltage at a frequency of 50 kHz and a peak-to-peak voltage of 8000 V. In order to improve the discharge stability, the power supply was triggered by a pulse generator (Thurbly instruments®), which modulated the sinusoidal voltage waveform with a square wave function. The modulated waveform was characterized by a plasma 'on' time of 4.5 ms and a period ($T_{on} + T_{off}$) of 25.5 ms, corresponding to a duty cycle of: $DC = T_{on}/(T_{on} + T_{off}) = 0.15$.

The applied voltage was measured using a Tektronix® P6015 high voltage probe, while the total current was recorded by an IonPhysics® current probe. Voltage and current waveforms were sampled by a Tektronix® TD 1002 digital oscilloscope. The total input power (P) dissipated into the plasma could then be determined by multiplying the duty cycle with the power, generated during one period of voltage (P_0), as shown in eq. (1).

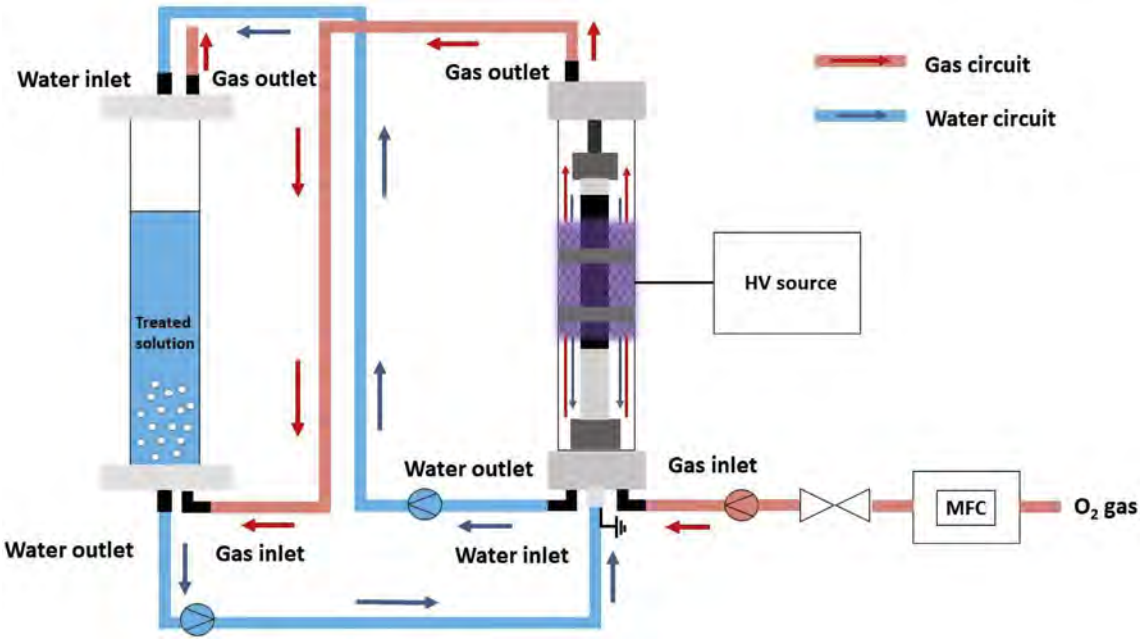

Fig. 1. Schematic representation of the plasma – ozonation reactor system, operated in batch-recirculation mode. The experimental system consists of a DBD plasma reactor (right) and a solution reservoir (left). All experiments were conducted using the following operational settings: feed gas: oxygen, gas flow rate: 1.0 slm, water flow rate: 56.3 mL min^{-1}, power: 40 W, ALA concentration: ± 1000 µg L^{-1}.

$$P = P_0 . DC \quad (1)$$

2.4. Reactor configurations

Experiments were conducted in the batch configuration to study the effect of (i) adsorption, (ii) adsorption combined with plasma treatment and (iii) plasma-ozonation on the removal of ALA. Prior to treatment, the solution reservoir was filled with 500 mL of a 1 mg L^{-1} ALA solution. The solution was continuously recirculated between the plasma chamber and the solution reservoir at a flow rate of 56.3 mL min^{-1}, corresponding to a residence time of 8.9 min and 2.09 s in the solution reservoir and the plasma chamber, respectively (Kovacevic et al., 2017). Details about the calculation method are given in Text S1 in the Supplementary Material. Aliquots of 20 mL were sampled from the reservoir at different time points (0, 2.5, 5, 10, 15, 20, 25, 30 min) and subjected to various analyses (see section 2.5 and Text S2 in the Supplementary Material). Taking samples during the batch experiments reduces the total solution volume under treatment. The error induced this way on the calculated reaction rate and EEO was determined to be less than 5%.

The plasma gas produced at the exhaust of the plasma chamber was either vented, or bubbled through the solution reservoir *via* a porous ceramic ozone dispenser during plasma-ozonation experiments. The removal of ALA by adsorption on the activated carbon textile was studied by recirculating the solution between both reactor chambers with the plasma switched off.

Single-pass experiments were conducted in the same experimental set-up and under similar operational settings as used for the batch-recirculating experiments. To allow the solution under treatment to pass through the plasma reactor only once, the reservoir was disconnected from the set-up, and the solution was continuously fed from the influent reservoir into the plasma chamber. ALA removal by adsorption on Zorflex® was measured after 10 s of operation. Subsequently, the plasma was switched on and samples were taken from the reactor outlet at identical time steps as in the batch experiments.

To evaluate the performance of the reactor system, the removal efficiency and energy consumption of each distinct process was determined. The removal efficiency (R) is defined as the ratio between the amount of ALA degraded in the reactor and the initial pollutant concentration (eq. (2)).

$$R = \frac{c_0 - c_t}{c_0}.100 \quad (2)$$

c_0 is the initial ALA concentration, and c_t the concentration detected in solution after a given treatment time. Energy consumption (calculated for 90% removal) is determined by the electrical energy per order (EE/O) figure-of-merit, and is defined by eqs. (3) and (4) for the batch-recirculating and the single-pass configuration, respectively (Bolton and Tumas, 1996).

$$EE / O_{batch} = \frac{P.t.1000}{V.60.\log(\frac{C_0}{C_f})} \quad (3)$$

$$EE \Big/ O_{single-pass} = \frac{P}{F.\log(\frac{C_0}{C_f})} \quad (4)$$

where t represents the treatment time and V is the solution volume.

2.5. Analytical techniques

The residual concentration of ALA in the treated samples was determined by gas chromatography-mass spectrometry (GC-MS). The methodology employed here is described in detail in our previous work (Wardenier et al., 2019; see also Fig. S1). Oxidation by-product analysis was performed by high-performance liquid chromatography coupled with a diode array UV detector and time-of-flight mass spectrometry (HPLC-TOF-MS; see Supplementary

Material for a complete description of the analytical procedures).

Gaseous O_3 in the exhaust gas stream, generated at the outlet of the plasma reactor and the solution reservoir was continuously monitored by a specially developed on-line ozone monitor (Text S2, section 2.1 in Supplementary Material).

In the liquid phase, EPR measurements were carried out in order to detect the presence of O, $^1O_2$ and O_3 (Gorbanev et al., 2016a,b; Gorbanev et al., 2018). For the quantification of hydrogen peroxide (H_2O_2), the titaniumoxysulphate method was used (Tarabová et al., 2018). Further details are provided in Text S2 (section 2.2) and Fig. S2 in the Supplementary Material.

3. Results & discussion

3.1. Alachlor removal kinetics

- Table 1 summarizes the ALA removal efficiency and energy consumption observed after adsorption, and adsorption combined with plasma treatment in the single-pass configuration. The percentage of removal and $EE/O_{single\text{-}pass}$ values, found at different time intervals after plasma ignition, along with a typical concentration profile is shown in Table S1 and Fig. S3 in the supplementary Material. In the single-pass experiment 39% removal was observed by adsorption alone as shown in Table 1 and Fig. S3. Although adsorption aided in the removal of ALA, it must be noted that the target compound decomposition did not occur: ALA was only transferred from the solution to the activated carbon surface. At longer exposure times, continuous adsorption of ALA on the activated carbon membrane would result in a decreased adsorption capacity, ultimately requiring a replacement of the carbon textile. Effective decomposition of ALA can only occur when activated carbon adsorption is combined with an advanced oxidation process, such as plasma treatment. Once the plasma was initiated, the ALA removal efficiency was increased reaching ca. 80% under steady-state conditions, corresponding to an energy cost of (19.4 ± 1.5) kWh m^{-3}, for an initial ALA concentration of 1 mg L^{-1}.

The increase in removal efficiency during the first 10 min of operation illustrates that the residence time of the ALA molecules in the discharge zone is much higher (i.e. several minutes) than the hydraulic residence time (HRT) of the solution, calculated from the assumption of a smooth laminar flow (2.09 s) (Kovacevic et al., 2017). According to the literature, steady-state concentrations are usually achieved within 3–5 times the hydraulic residence time (HRT) (Gerrity et al., 2010; Ajo et al., 2016). Following this line of thought, the ALA residence time in the plasma reactor is estimated to be in the range 2–3 min. Probably, the difference in residence time between the solution and the ALA molecules in the discharge zone is due to the continuous process of adsorption and desorption of ALA on the carbon surface when passing through the reactor. This in turn enhances the probability of interactions between the plasma-generated oxidants and the alachlor molecules adsorbed on the activated carbon textile.

The removal of ALA by adsorption, plasma-treatment, and plasma-ozonation during treatment in the batch-recirculating configuration is shown in Fig. 2. Similarly to the single-pass configuration, lowest removal efficiency was found for ALA adsorption on Zorflex®, accounting for 88.2% removal after 30 min of treatment. A faster elimination of ALA was found during plasma treatment and plasma – ozonation, where complete elimination was observed after 30 and 15 min of operation, respectively. When present in low concentrations (<100 mg L^{-1}) the elimination of organic compounds from water, with advanced oxidation processes (AOPs) or plasma treatment obeys a pseudo-first order kinetics (Bolton and Tumas, 1996). Hence, the rate law describing pollutant decomposition reads as (eq. (5)):

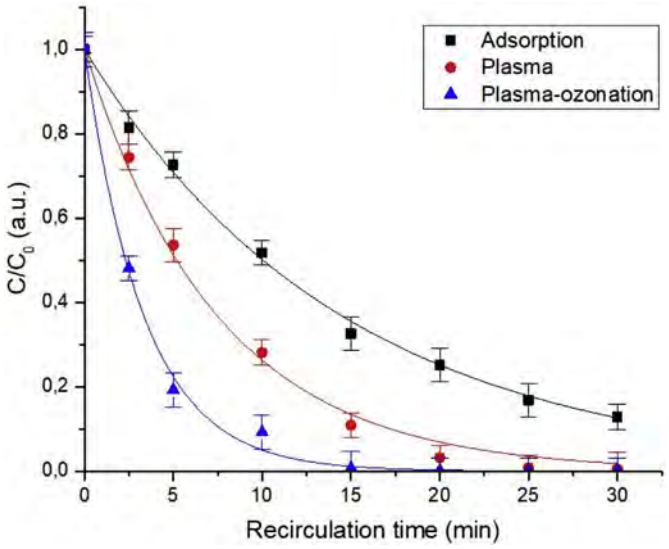

Fig. 2. Removal efficiency of ALA in the batch-recirculation setup. Experimental conditions were similar in both reactor configurations (O_2 gas flow rate: 1 slm, water flow rate: 56.3 mL min^{-1}, initial ALA concentration: 1008 μg L^{-1}, power: 40.7 W and 39.4 W).

$$\frac{dC}{dt} = -k.C \quad (5)$$

With C the pollutant concentration (mol/l), t treatment time (s) and k the pseudo-first order rate constant (s^{-1}). The solution of eq. (5) ($C = C_0.e^{-k.t}$) suggests an exponential decay in alachlor concentration as a function of treatment time, which is consistent with the shape of the alachlor decomposition profile shown in Fig. 2. The pseudo-first order rate constant was obtained by fitting experimental data shown in Fig. 2 to eq. (5) by means of nonlinear least squares regression, following the Levenberg-Marquardt algorithm.

To check the assumption of alachlor decomposition described by a pseudo first-order kinetics, Table S2 in the Supplementary Material compares the computed rate constants and correlation coefficients (R^2) obtained from the fitting of the data with a zeroth order, pseudo-first order and second order kinetic model. A satisfactory agreement was found between the experimental data and the model predictions obtained from the pseudo-first order kinetic model ($R^2 > 0.998$ for the three fittings), whereas the R^2 values were smaller for the zeroth second order kinetic models ($R^2 < 0.94$). This justifies the use of a pseudo-first order kinetic model for the accurate prediction of the alachlor decomposition.

Table 1
Removal efficiency (R) and energy cost ($EE/O_{single\text{-}pass}$) observed in single-pass mode, after one pass through the reactor. All experimental conditions are identical to the ones mentioned in the caption of Fig. 1. The removal efficiency and EE/O values were calculated using eqs. (2) and (4), respectively.

Time (min)	Treatment condition	R (%)	$EE/O_{single\text{-}pass}$ (kWh m^{-3})
0.1	Adsorption alone	39.1%	–
2.5	Adsorption + plasma (steady-state not reached)	52.4%	22.1
30	Adsorption + plasma (steady-state)	78.4%	19.7

The rate constant ($k = 0.299 \pm 0.0102$ min^{-1}) obtained in the plasma-ozonation setup is more than twice as high compared to the value found during plasma treatment alone ($k = 0.134 \pm 0.0055$ min^{-1}). Based on the kinetic data presented in Fig. 2, the energy consumption is found to be 23.4 kWh m^{-3} and 10.4 kWh m^{-3} for the elimination of ALA by plasma and plasma-ozonation, respectively. Thus, it is evident that the bubbling of the excess plasma gas (mainly containing ozone) throughout the solution reservoir is beneficial to achieve a better removal efficiency, and a lower energy consumption.

3.2. Production of reactive species by plasma

Plasma-assisted decomposition of organic compounds is typically a complex process, that involves the participation of multiple oxidising reagents, such as reactive oxygen species (ROS). In a gas phase plasma sustained in a humid O_2 atmosphere, collisions between the electrons and the gas molecules (O_2, H_2O) initiate the production of oxidising species including various radicals ($HO^{\bullet}$, $HO_2^{\bullet}$, O, H), excited species ($^1O_2$), neutral molecules (O_3, H_2O_2, H_2) and charged ions (O^+, O^{2+}, O^{4+}, HO^+, H^+, H^-, HO^-, O^-, O^{2-}, O^{4-}) through a series of chemical reactions (Bradu et al., 2017; Jiang et al., 2014).

Reactive species generated in the gas phase then diffuse in the liquid, where they initiate secondary reactions. For reactor systems that combine plasma treatment with activated carbon adsorption, organic pollutant elimination can take place simultaneously in the plasma-liquid interface, the bulk liquid and on the catalyst surface. A plausible pathway, describing the decomposition of organic compounds was put forward by Jiang et al. (2014) and is summarized in reactions R1-R8.

First, micropollutants present in the bulk liquid phase diffuse from the bulk liquid to the activated carbon surface, where a fraction of the initial ALA concentration is adsorbed (R.1). The adsorption efficiency depends on the nature of the target compound, as described in Vanraes et al. (2018). From the results obtained from single-pass experiment summarized in Table 1, it could be deduced that about 49% is removed from the solution by adsorption on the Zorflex® textile, after one pass through the reactor. Hereby, the accumulation of ALA at the active carbon textile results in a local micropollutant concentration in the region near the plasma-liquid interface, resulting in a higher probability for interactions with the plasma-generated oxidants present in the liquid-phase. Furthermore, it is important to stress that activated carbon itself also catalyses the decomposition of long-living oxidants (O_3, H_2O_2), present in the bulk liquid, through a series of reactions (R.2 – R.7), generating highly reactive radicals in solution and attached to the adsorption material, which can contribute to the elimination of ALA. This leads to the self-regeneration of activated carbon and thus prolongs the lifetime of the activated carbon textile. Indeed, several works have suggested the use of plasma technology for the regeneration of activated carbon (Gushchin et al., 2018; Jiang et al., 2014; Qu et al., 2009; Tang et al., 2018).

$$AC + M \rightarrow AC - -M \quad (R.1)$$

$$O_3 + H - AC - H \rightarrow AC - O + H_2O_2 \quad (R.2)$$

$$O_3 + AC - OH \rightarrow {}^{\bullet}O_2 - AC + HO^{\bullet} \quad (R.3)$$

$$O_3 - AC \rightarrow O_2 + {}^{\bullet}O - AC \quad (R.4)$$

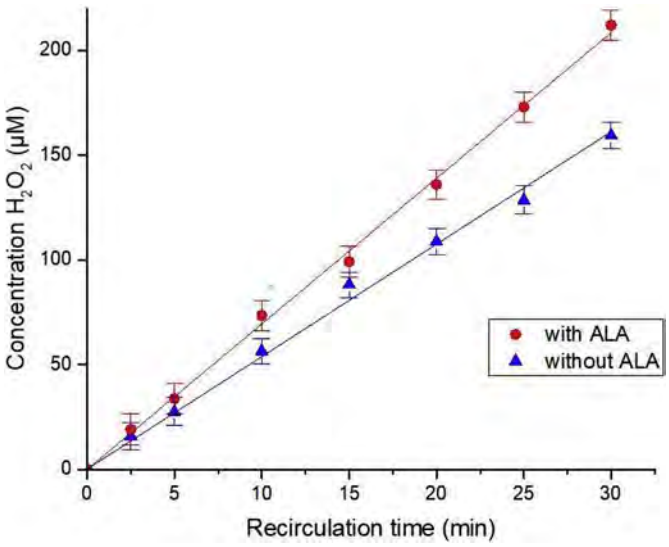

Fig. 3. Production of H_2O_2 in the presence and absence of ALA, for the batch-recirculating configuration.

$$O_3 - AC + O - AC \rightarrow O_2^{\bullet -} + O^{\bullet} + AC \quad (R.5)$$

$$AC + H_2O_2 \rightarrow AC^+ + HO^- + HO^{\bullet} \quad (R.6)$$

$$AC^+ + H_2O_2 \rightarrow AC + H^+ + HO_2^{\bullet} \quad (R.7)$$

$$AC - - M + HO^{\bullet} \rightarrow AC + P \quad (R.8)$$

To elucidate the role that oxidising species can play in the elimination of ALA, the contribution of various chemical oxidants to ALA removal was studied in the following sections.

3.2.1. Hydrogen peroxide in batch-mode

Fig. 3 illustrates the formation of H_2O_2 in the liquid phase for the batch-recirculating configuration. A linear increase of H_2O_2 concentration was observed in deionized water, reaching a concentration of ca. 220 μM, while a higher amount (272 μM) of H_2O_2 was formed in the presence of ALA, after 30 min of treatment. A similar finding, i.e. a higher concentration of H_2O_2 in the presence of an organic compound dissolved in deionized water was previously reported in a pulsed corona discharge (Magureanu et al., 2016).

It is well-documented that hydrogen peroxide is mainly formed from radical-radical recombination reactions in the plasma-treated liquid (R.9–10). Following this consideration, the detection of H_2O_2 in solution indirectly confirmed the presence of radical species ($HO^{\bullet}$, $HO_2^{\bullet}$). As an additional source, in gas phase discharge, part of the H_2O_2 found in the liquid might be attributed to the direct transfer of H_2O_2 from the gas phase plasma to the liquid, due to its high Henry's constant ($H^{CC} = 1.92 \times 10^6$) (Lietz and Kushner, 2016; Heirman et al., 2019).

$$HO^{\bullet} + HO^{\bullet} \rightarrow H_2O_2 \quad (R.9)$$

$$HO_2^{\bullet} + HO_2^{\bullet} \rightarrow H_2O_2 + O_2 \quad (R.10)$$

Franclemont et al. (2015) reported H_2O_2 concentrations up to 800 μM in a pulsed corona discharge directly in the liquid, while Sarangapani et al. (2017) observed a smaller amount of H_2O_2 (490 μM) in a DBD reactor fed with air. Further, Kovacevic et al. (2017) showed that the production of H_2O_2 in a liquid film

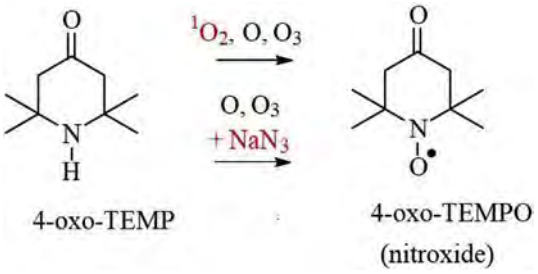

Fig. 4. Oxidation of 4-oxo-TEMP to 4-oxo-TEMPO by the plasma-created ROS. Sodium azide (NaN_3) acts as a scavenger for singlet oxygen($^1O_2$).

reactor depends on the nature of the feed gas. The authors observed the largest H_2O_2 concentration in pure Ar (588 μM). On the contrary a slightly smaller concentration of H_2O_2 could be detected during air plasma treatment (441 μM). The latter is explained by the consumption of H_2O_2 due to the reaction with nitrite (NO_2^-) which takes place in an acidic environment.

The efficiency of H_2O_2 generation in plasma reactor is often expressed by the H_2O_2 energy yield (g.kWh^{-1}). In the review of Locke and Shih (2011) H_2O_2 energy yields were summarized for a variety of plasma reactors. H_2O_2 energy yields up to 80 g kWh^{-1} were reported for reactor configurations where the plasma was generated in the liquid while in most DBD reactors, energy yield was calculated to be around 2.70 g kWh^{-1}. In this study, the H_2O_2 yield was substantially lower. For instance, in the absence of ALA, the H_2O_2 production efficiency was 49.2 × 10^{-2} g kWh^{-1}. Likely, a part of H_2O_2 formed in the bulk liquid is decomposed on the activated carbon textile, in agreement with reactions R.6 – R.7. Note that, according to this reaction mechanism, H_2O_2 is converted into $HO^\bullet$ and $HO_2^\bullet$ radicals, which have a higher reactivity with organic pollutants, and might thus be beneficial to achieve a faster pollutant decomposition.

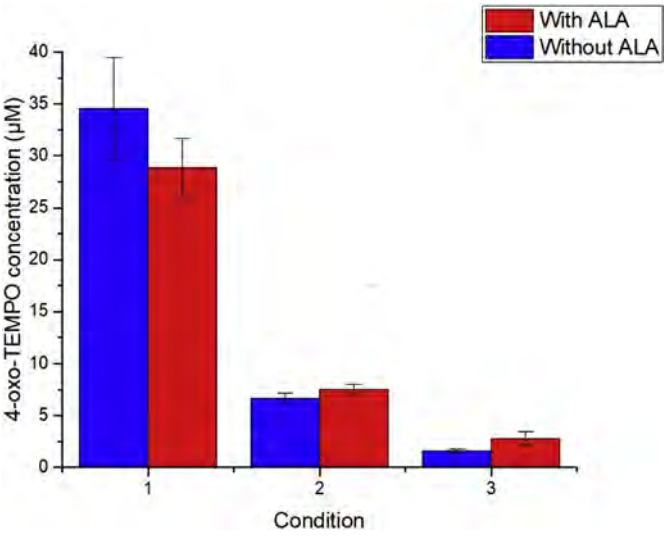

Fig. 5. Concentrations of 4-oxo-TEMPO formed in the oxidation reaction of 4-oxo-TEMP by O/O_3/$^1O_2$ after 15 min of treatment in the single-pass configuration with and without ALA. Conditions: 1) 5 mM 4-oxo-TEMP; 2) 5 mM 4-oxo-TEMP + 5 mM NaN_3; 3) post-treatment 5 mM 4-oxo-TEMP. The error bars show the standard deviation calculated from 4 experiments. A Student's t-test revealed no significant difference in 4-oxo-TEMPO concentration in the presence and absence of ALA, for all conditions ($p < 0.05$).

3.2.2. Electron paramagnetic resonance measurements for assessing oxygen-derived reactive species

The presence of oxygen-derived reactive species such as ozone (O_3), atomic oxygen ($O^\bullet$), and singlet oxygen ($^1O_2$) was assessed in the liquid, using electron paramagnetic resonance (EPR) spectroscopy with a spin trap 4-oxo-2,2,6,6-tetramethyl-1-piperidine (4-oxo-TEMP). Upon the oxidation of the amine group by these species, a stable nitroxide radical 4-oxo-2,2,6,6-tetramethyl-1-piperidine *N*-oxyl (4-oxo-TEMPO) is formed, as illustrated in Fig. 4 (Elg et al., 2017; Privat-Maldonado et al., 2018; Takamatsu et al., 2014), and its concentration is measured using EPR as described in section 2.5 and Text S2. It is worth mentioning that other potentially present species such as hydroxyl and superoxide radicals, as well as hydrogen peroxide, were shown to not oxidise piperidines in plasma-liquid systems (Gorbanev et al., 2016a,b). It also must be noted that spin trapping does not provide quantitative information about the total concentration of a reactive species present in the liquid (Privat-Maldonado et al., 2018; Rezaei et al., 2018). However, the changes in the concentration of the formed 4-oxo-TEMPO directly correlate with the changes in the concentrations of the initially available free ROS (Elg et al., 2017; Gorbanev et al., 2016a,b).

The presence of various ROS was first analysed for the single-pass experiments, 5 mM solutions of 4-oxo-TEMP in water with and without ALA were passed through the plasma chamber once. In this case, the concentration of 4-oxo-TEMPO correlates to the sum of concentration of initially available oxidising species (O, $^1O_2$, O_3) in the liquid after plasma exposure (condition 1).

To elaborate on the individual contributions of ROS to the oxidation of 4-oxo-TEMP, two additional sets of experiments were carried out. First, the experiments were repeated with solutions containing 50 mM of added sodium azide (a quencher of $^1O_2$ at neutral pH (Elg et al., 2017; Gorbanev et al., 2016a,b; Takamatsu et al., 2014)) (condition 2). Second, solutions containing only ALA were treated, and 5 mM 4-oxo-TEMP was added to the aqueous solution immediately after the sample collection, with a maximal time delay of about 5 s (condition 3). Taking into account the short lifetime of oxygen species such as $^1O_2$ and O in aqueous solutions, the formation of 4-oxo-TEMPO in these experiments can be assigned to the presence of O_3 in the treated solutions.

The results for both solutions with and without ALA are shown in Fig. 5. The formation of 4-oxo-TEMPO up to a concentration of ca. 35 μM clearly established the presence of ROS in the plasma-treated solution. To explore the potential difference in the concentration of 4-oxo-TEMPO detected in the solution, a Student's t-test was conducted. Within the accuracy of the measurements, the concentration of 4-oxo-TEMPO under all three conditions was found to be similar in the presence and absence of ALA ($p > 0.05$). In other words, the presence of ALA does not dramatically affect the concentration of the formed 4-oxo-TEMPO and therefore the concentration of available ROS. This is likely due to the large difference (three orders of magnitude) in the initial concentrations of ALA and 4-oxo-TEMP.

The addition of NaN_3 to the initial solution (condition 2) strongly reduced the concentration of 4-oxo-TEMPO. It was shown that NaN_3 does not affect the concentration of the formed nitroxide in the plasma-liquid systems when O_3 and O (without $^1O_2$) are both present in the liquid (Elg et al., 2017; Gorbanev et al., 2016a,b). Therefore, the reduced formation of 4-oxo-TEMPO when NaN_3 was added to the solution, is attributed to the scavenging of $^1O_2$. This means that $^1O_2$ is created in the gas phase plasma, and further diffused into the liquid, where it contributes to the degradation of ALA.

A substantially lower (but still detectable) amount of 4-oxo-TEMPO was also formed when 4-oxo-TEMP was added to the

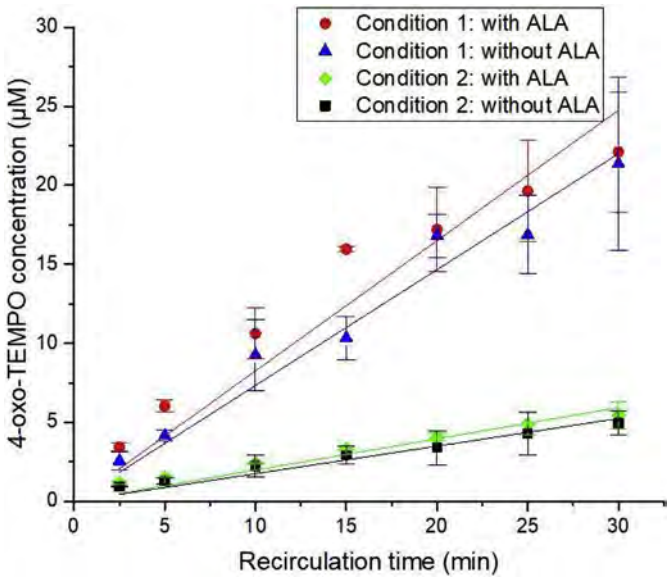

Fig. 6. Concentration of 4-oxo-TEMPO in 500 mL solution in the recirculated system. Condition 1: 4-oxo-TEMP (5 mM) added to the initial solution. Condition 2: 4-oxo-TEMP (5 mM) and NaN_3 (5 mM) added to the initial solution. The error bars show the standard deviation obtained from 2 experiments. A Student's t-test revealed no significant difference in 4-oxo-TEMPO concentration in the presence and absence of ALA, for all conditions ($p < 0.05$).

aqueous solutions collected from the reactor outlet. Considering the short lifetime of O and $^1O_2$ in aqueous solutions, the formation of 4-oxo-TEMPO in this experiment shows the presence of residual O_3 in the liquid. This proves that O_3 is present in the treated water even during the single pass configuration (e.g. without using additional ozonation).

Further, experiments were performed in batch mode, in which the liquid was continuously recirculated between the solution reservoir and the plasma chamber (see Fig. 1 above). In these experiments, 500 mL of the solution was continuously passed through the plasma reactor at a flow rate of 56.3 mL min^{-1}, and samples were taken directly from the solution reservoir. The concentration of 4-oxo-TEMPO was measured in the analysed samples for the same experimental conditions as used in the single-pass experiments, and is shown in Fig. 6.

Under conditions 1 and 2, the concentration of the formed 4-oxo-TEMPO increased near-linearly within the experimental timeframe (Fig. 6). Additionally, an increase in the amount of the residual O_3 (condition 3) was noticed as presented in Fig. S4 in the Supplementary Material. No significant difference was observed between the solution with and without ALA, consistently with the results obtained in the single-pass experiments (Fig. 5). Furthermore, in Fig. 6, the low concentration of the formed 4-oxo-TEMPO after 2.5 and 5 min can in part be explained by the dilution of the solution that passed through the reactor with the rest of the solution in the reservoir. Alternatively, the lower concentration of 4-oxo-TEMPO detected in batch mode can also be attributed to enhanced degradation of the formed nitroxide (N–O•) radical moiety in the 4-oxo-TEMPO molecule at prolonged plasma exposure times. The nitroxide group is prone to decay caused by e.g. HO• radicals in plasma-liquid systems (Gorbanev et al., 2016b). At longer exposure times, H_2O_2 was accumulating in the liquid solution, as presented earlier in Fig. 3. At high concentrations, H_2O_2 can react with atomic O (Elg et al., 2017; Hefny et al., 2016; Verlackt et al., 2017) or O_3 (Merenyi et al., 2010), generating large amount of additional HO• radicals in the liquid.

3.3. Oxidation products

As mentioned above, several oxidising species might be generated during plasma treatment and therefore potentially be involved in the decomposition of alachlor. It has been reported that the hydroxyl radical (HO•) preferentially reacts with organic compounds through three major reaction pathways, being (i) the abstraction of a hydrogen atom, ii) the electrophilic addition of a HO• radical to multiple bonds, and iii) electron transfer reactions. To the best of our knowledge, no information is available in the literature concerning the reaction mechanisms of organic compounds with other oxidants (i.e. O or $^1O_2$). Therefore, it is not possible to assign the detection of a certain by-product to the presence of a specific oxidant in solution.

For the reactor operated in batch-recirculation mode, the oxidation by-product analysis has already been reported in our previous work (Vanraes et al., 2018). For oxygen plasma, four types of oxidation steps were observed:

- hydroxylation;
- addition of a double bonded oxygen;
- dealkylation;
- dechlorination.

As shown in Table S3 in the Supplementary Material, most of the by-products that were identified in the previous study (when plasma was ignited in either O_2 or air; Vanraes et al. (2018)) are also found in the present study for treatment with O_2 plasma in the single-pass flow-through setup. The exception was dechlorinated ALA (2D), demethylated ALA with and without the addition of a double bonded oxygen (3 B and 3U), and four compounds formed through one or more hydroxylation and/or oxygen addition steps (3I, 3R, 3S and 3Z). A proposed reaction pathway in the plasma reactor is given in Fig. 7. As expected, the four oxidation steps are observed in the single-pass configuration in most identified by-products.

Comparison of the ion abundances in the HPLC-TOF-MS analysis indicates a majority of hydroxylated by-products, such as the five monohydroxylated isomers K (see Fig. 8). Compounds formed through the addition of double bonded oxygen make the next most abundant group, including the R and E isomers with one and two added oxygen atoms, respectively. This stands in contrast with the results for treatment in the batch reactor configuration, where by-products with a double bonded oxygen dominated in the analysis results (see Fig. 8(b)). Especially one of the R isomers, i.e. R', was found in a remarkably high abundance. It should be noted that the mentioned abundance values are only indicative for the corresponding by-product concentration. Although the HPLC-TOF-MS method is expected to have a similar sensitivity to compounds with a similar chemical structure, a calibration for each of the products would be required to obtain exact concentrations. Therefore, the abundance values can be used to get an idea of the order of magnitude of the concentration, but should not be understood as exact concentration values.

Second, the abundance of any compound in Fig. 8 for the batch reactor configuration corresponds to the sample with its highest abundance, i.e. taken after at least 2.5 min of treatment. In contrast, the HRT of the solution in the plasma reactor is about 2 s. This retention time applies to the plasma reactor in the batch configuration as well. Keeping this in mind, the high abundance of R′ in the batch reactor relative to the single-pass configuration cannot be explained solely with the processes in the plasma reactor and is probably mainly due to the chemistry in the ozonation chamber. R' has indeed been reported as the main ALA oxidation by-product for ozonation and the peroxone process (Qiang et al., 2010), which are

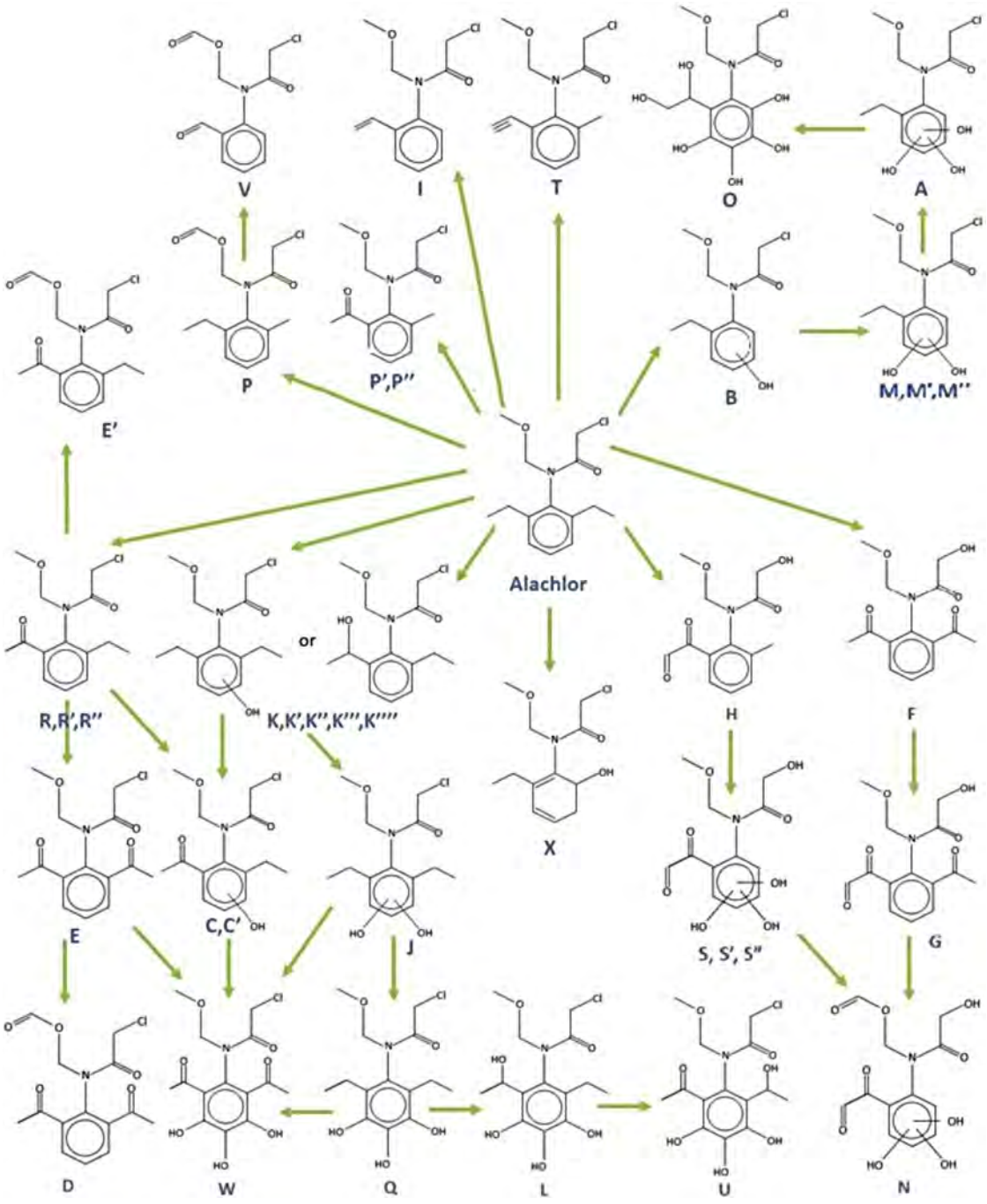

Fig. 7. Proposed reaction pathway for ALA decomposition with oxygen plasma in the single-pass configuration. The structural formulas of the detected by-products (e.g. the location of hydroxylation or addition of a double bonded oxygen) is often not exactly known, but are drawn according to our best interpretation of the experimental data.

expected to be the main oxidation processes in the solution reservoir. This seems to imply that the addition of a double bonded oxygen is generally a more common mechanism than hydroxylation during ALA oxidation in ozonation or the peroxone process, which can explain the observed difference in their prevalence between the single-pass and batch experiments.

Next to hydroxylation and addition of a double bonded oxygen, dechlorination and dealkylation of the ALA side chains is observed in all studied conditions, albeit to a lower degree (Fig. 8). Remarkably, a few by-products are measured in the single-pass reactor configuration that cannot be explained solely with these four types of oxidation steps. The by-products I and T, for instance, require an additional step with hydrogen subtraction and likely the formation of a double or triple bond between two carbons. Further, as seen in Table S3, the mass spectrum of by-product X displays the same dissociation pattern as ALA. In this pattern, the first daughter ion is formed with the release of a CH_3OH fragment, which sequentially results in the second daughter ion by the elimination of a C_2HClO fragment. Since both fragments originate from the N-substituted branch, this branch is identical for both molecules. Therefore, the oxidation mechanisms that led to by-product X took place at the other part of the molecule. This, however, implies that the chemical

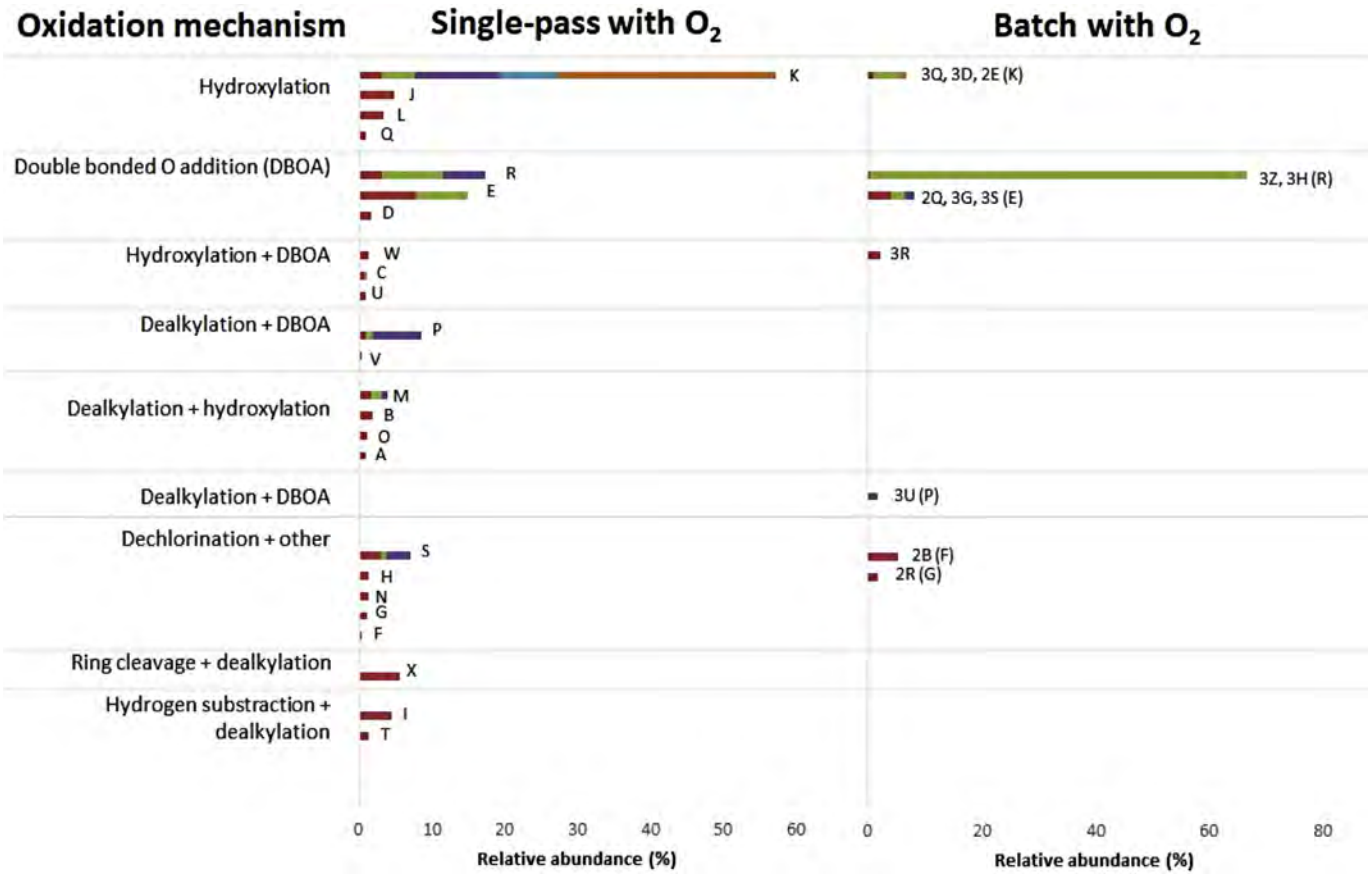

Fig. 8. Relative abundance of each oxidation by-product on removal of ALA in the a) single-pass configuration and b) the batch configuration. Each color represents a different isomer. By-product names that start with a cypher refer to the nomenclature in our previous work (Vanraes et al., 2018). Each color and its corresponding length represents a different isomer and its measured abundance, where the sequence red, green, purple, blue and orange indicates the order in which the isomers appeared in the chromatogram. (For interpretation of the references to color in this figure legend, the reader is referred to the Web version of this article.)

formula of X cannot be explained with an aromatic ring, as it has a lower degree of unsaturation. In other words, the aromatic structure has been lost in X and perhaps ring cleavage has taken place. This is a very important finding, since the loss of aromaticity, although expected to occur (Qiang et al., 2010), is not frequently observed in advanced oxidation processes. Noteworthy, some of the other by-products in Fig. 8 also may have lost their aromatic structure, for instance if the combination of ring breaking and the addition of a double bonded oxygen has instead been identified as a hydroxylation step (the HPLC-TOF-MS measurements can often not distinguish between both types of isomers).

3.4. Influence of additional ozonation

In the plasma discharge, ozone is formed from a three-body reaction involving, atomic oxygen (O) and molecular oxygen (O_2) (R. 11).

$$O^{\bullet} + O_2 + M \rightarrow O_3 + M \quad (R.11)$$

Additional plasma gas bubbling into the solution reservoir appeared to be beneficial for the removal efficiency and energy consumption, as shown above in Fig. 2. To assess the contribution of O_3 to the degradation of ALA, the amount of gaseous O_3 generated at the outlet of the plasma reactor and the solution reservoir was measured. The concentration of O_3 detected at the exhaust of the solution reservoir, was found to be lower (7738 ± 8 mg m^{-3}) as compared to the amount of O_3 produced at the outlet of the plasma reactor (8789 ± 26 mg m^{-3}). At steady-state conditions, the total O_3 consumption in the ozonation chamber was determined by subtracting the amount of ozone measured at the exhaust of the ozonation chamber from the gaseous ozone concentration detected at the outlet of the plasma chamber. This confirmed that in the plasma-ozonation setup about 1051 mg m^{-3} O_3 was dosed in the solution reservoir, where it reacted with the pesticide and its by-products, or other oxidative species present in the liquid generating additional radicals (such as e.g. a reaction between H_2O_2 and O_3 (Merenyi et al., 2010; Wang et al., 2018). The production of hydroxyl radicals during the decomposition of O_3 is particularly advantageous, due to their extremely high, nearly diffusion-controlled reaction rate constants with most organic pollutants (Wols and Hofman-Caris, 2012).

4. Conclusion

In this work, the removal of a chlorinated pesticide (ALA) from deionized water was studied in a pulsed DBD plasma reactor, combining plasma treatment with adsorption and additional ozonation. The contribution of each distinct removal process was evaluated and a comparison in reactor performance between a single-pass and batch-recirculation configuration was made. In both configurations, the lowest removal efficiency was observed when ALA removal was attempted with activated carbon adsorption alone. In the single-pass experiments, about 39% was removed after one pass through the reactor, and more than 80% of ALA was

adsorbed after 30 min of treatment in batch recirculation mode. With regard to the energy efficiency of ALA removal during plasma treatment in combination with activated carbon adsorption, a slightly better energy cost is obtained in the single-pass configuration ($EE/O_{single\text{-}pass} = 19.4\ kWh\ m^{-3}$) than in batch-recirculation mode ($EE/O_{batch} = 23.4\ kWh\ m^{-3}$).

To evaluate the role of aqueous oxidants on the decomposition of ALA, the production of various active species (H_2O_2, O_3, $^1O_2$, O) was monitored by UV–Vis spectrophotometry and EPR spectroscopy. From EPR analysis, the presence of O, $^1O_2$ and O_3 was identified in the plasma-treated solution, and could thus contribute to the decomposition of alachlor. Interestingly, the H_2O_2 concentration formed in the reactor (220 μM) was slightly smaller than the amount of H_2O_2 usually detected (i.e. up to a few mM) during plasma treatment in a DBD. This could be attributed to the decomposition of H_2O_2 on the catalyst surface. Future experimental and computational (micro-kinetic) studies could provide more details of the exact mechanism.

The reaction intermediates of ALA in the single-pass configuration are mainly formed through six major mechanisms, including various hydroxylation, dealkylation, and dechlorination reactions, as well as the loss of aromaticity. Finally, the abundant production of O_3 in the plasma suggested that the process could be enhanced by bubbling the plasma exhaust gas into the solution reservoir. The energy cost was almost two times lower with the plasma exhaust gas bubbling through the solution ($EE/O = 10.4\ kWh\ m^{-3}$) when compared with plasma treatment alone ($EE/O = 23.4\ kWh\ m^{-3}$) at 90% ALA removal.

Declaration of interests

The authors declare that they have no known competing financial interests or personal relationships that could have appeared to influence the work reported in this paper.

Acknowledgements

This work was financially supported by the PlasmaTex project IWT 1408/2 and the European Marie Sklodowska-Curie Individual Fellowship within Horizon2020 ('LTPAM', grant no. 743151). This research was initiated within the LED H2O project which is financially supported by the Flemish Knowledge Centre Water (Vlakwa).

Appendix A. Supplementary data

Supplementary data to this article can be found online at https://doi.org/10.1016/j.watres.2019.06.022.

References

Ajo, P., Krzymyk, E., Preis, S., Kornev, I., Kronberg, L.A., Louhi-Kultanen, M., 2016. Pulsed corona discharge oxidation of aqueous carbamazepine micropollutant. Environ. Technol. 37 (16), 2072–2081. http://doi.org/10.1080/09593330.2016.1141236.

Badriyha, B.N., Ravindran, V., Den, W., Pirbazari, M., 2003. Bioadsorber efficiency, design, and performance forecasting for alachlor removal. Water Res. 37 (17), 4051–4072. http://doi.org/10.1016/S0043-1354(03)00266-5.

Bolton, J.R., Tumas, W., 1996. Figures of merit for the technical development and application of advanced oxidation process. J. Adv. Oxid. Technol. 1 (1), 0–11. https://doi.org/10.1515/jaots-1996-0104.

Bradu, C., Magureanu, M., Parvulescu, V.I., 2017. Degradation of the chlorophenoxyacetic herbicide 2,4-D by plasma-ozonation system. J. Hazard Mater. 336, 52–56. https://doi.org/10.1016/j.jhazmat.2017.04.050.

Eggen, R.I.L., Hollender, J., Joss, A., Schärer, M., Stamm, C., 2014. Reducing the discharge of micropollutants in the aquatic environment: the benefits of upgrading wastewater treatment plants. Environ. Prog. 48 (14), 7683–7689. https://doi.org/10.1021/es500907n.

Elg, D.T., Yang, I., Graves, D.B., 2017. Production of TEMPO by O atoms in atmospheric pressure non-thermal plasma – liquid interactions. J. Phys. D Appl. Phys. 50 (47), 472501. http://doi.org/10.1088/1361-6463/aa8f8c.

Franclemont, J., Fan, X., Thagard, S.M., 2015. Physicochemical mechanisms of plasma-liquid interactions within plasma channels in liquid. J. Appl. Phys. 48, 424004, 10.1088/0022-3727/48/424004.

Gerrity, D., Stanford, B.D., Trenholm, R.A., Snyder, S.A., 2010. An evaluation of a pilotscale nonthermal plasma advanced oxidation process for trace organic compound degradation. Water Res. 44 (2), 493–504. http://doi.org/10.1016/j.watres.2009.09.029.

Gorbanev, Y., O'Connell, D.O., Chechik, V., 2016a. Non-thermal plasma in contact with water: the origin of species. Chemistry 22 (10), 3496–3505. http://doi.org/10.1002/chem.201503771.

Gorbanev, Y., Stehling, N., O'Connell, D., Chechik, V., 2016b. Reactions of nitroxide radicals in aqueous solutions exposed to non-thermal plasma : limitations of spin trapping of the plasma induced species. Plasma Sources Sci. Technol. 25 (5), 055017. http://doi.org/10.1088/0963-0252/25/5/055017.

Gorbanev, Y., Verlackt, C.C.W., Tinck, S., Tuenter, E., Foubert, K., Cos, P., Bogaerts, A., 2018. Combining experimental and modelling approaches to study the sources of reactive species induced in water by the COST RF plasma jet. Phys. Chem. Chem. Phys. 20 (4), 2797–2808. http://doi.org/10.1039/C7CP07616A.

Gushchin, A.A., Grinevich, V.I., Gusev, G.I., Kvitkova, E.Y., Rybkin, V.V., 2018. Removal of oil products from water using a combined process of sorption and plasma exposure to DBD. Plasma Chem. Plasma Process. 38 (5), 1021–1033. http://doi.org/10.1007/s11090-018-9912-4.

Hefny, M.M., Pattyn, C., Lukes, P., Benedikt, J., 2016. Atmospheric plasma generates oxygen atoms as oxidizing species in aqueous solutions. J. Phys. D Appl. Phys. 49 (40), 404002. http://doi.org/10.1088/0022-3727/49/40/404002.

Heirman, P., Van Boxem, W., Bogaerts, A., 2019. Reactivity and stability of plasma-generated oxygen and nitrogen species in buffered water solution: a computational study. Phys. Chem. Chem. Phys. Accepted manuscript https://doi.org/10.1039/C9CP00647H.

Ikehata, K., El-din, M.G., 2005. Aqueous pesticide degradation by ozonation and ozone-based advanced oxidation processes: a review (Part I). Ozone: Sci. Eng. 27 (2), 37–41. http://doi.org/10.1080/01919510590925220.

Jiang, B., Zheng, J., Qiu, S., Wu, M., Zhang, Q., Yan, Z., Xue, Q., 2014. Review on electrical discharge plasma technology for wastewater remediation. Chem. Eng. J. 236, 348–368. http://doi.org/10.1016/j.cej.2013.09.090.

Köck-Schulmeyer, M., Villagrasa, M., López de Alda, M., Céspedes-Sánchez, R., Ventura, F., Barceló, D., 2013. Occurrence and behavior of pesticides in wastewater treatment plants and their environmental impact. Sci. Total Environ. 458–460, 466–476. https://doi.org/10.1016/j.scitotenv.2013.04.010.

Kovacevic, V.V., Dojcinovic, B.P., Jovic, M., Roglic, G.M., Obradovic, B.M., Kuraica, M.M., 2017. Measurement of reactive species generated by dielectric barrier discharge in direct contact with water in different atmospheres. J. Phys. D Appl. Phys. 50 (15), 155205. http://doi.org/10.1088/1361-6463/aa5fde.

Lietz, A.M., Kushner, M.J., 2016. Air plasma treatment of liquid covered tissue : long timescale chemistry. J. Phys. D Appl. Phys. 49 (42), 425204. http://doi.org/10.1088/0022-3727/49/42/425204.

Locke, B.R., Shih, K.-Y., 2011. Review of the methods to form hydrogen peroxide in electrical discharge plasma with liquid water. Plasma Sources Sci. Technol. 20 (3), 034006. http://doi.org/10.1088/0963-0252/20/3/034006.

Luo, Y., Guo, W., Ngo, H.H., Nghiem, L.D., Hai, F.I., Zhang, J., Liang, S., Wang, X.C., 2014. A review on the occurrence of micropollutants in the aquatic environment and their fate and removal during wastewater treatment. Sci. Total Environ. 473–474, 619–641. http://doi.org/10.1016/j.scitotenv.2013.12.065.

Magureanu, M., Dobrin, D., Bradu, C., Gherendi, F., Mandache, N.B., Parvulescu, V.I., 2016. New evidence on the formation of oxidizing species in corona discharge in contact with liquid and their reactions with organic compounds. Chemosphere 165, 507–514. https://www.doi.org/%2010.1016/j.chemosphere.2016.09.073.

Marican, A., Durán-lara, E.F., 2018. A review on pesticide removal through different processes. Environ. Sci. Pollut. Control Ser. 25, 2051–2064. https://doi.org/10.1007/s11356-017-0796-2.

Merenyi, G., Lind, J., Naumov, S., Von Sonntag, C., 2010. Reaction of ozone with hydrogen peroxide (peroxone process): a Revision of current mechanistic concepts based on thermokinetic and quantum-chemical considerations. Environ. Sci. Technol. 44 (9), 3505–3507. https://doi.org/10.1021/es100277d.

Oturan, M.A., Aaron, J., 2014. Advanced oxidation processes in water/wastewater treatment: principles and applications. A Review. Crit. Rev. Environ. Sci. Technol. 44 (23), 2577–2641. http://doi.org/10.1080/10643389.2013.829765.

Privat-Maldonado, A., Gorbanev, Y., Connell, D.O., Vann, R., Chechik, V., Van der Woude, M.W., 2018. Nontarget biomolecules alter macromolecular changes induced by bactericidal low-temperature plasma. IEEE Transactions on Radiation and Plasma Medical Sciences 2 (2), 121–128. https://doi.org/10.1109/TRPMS.2017.2761405.

Qiang, Z., Liu, C., Dong, B., Zhang, Y., 2010. Degradation mechanism of alachlor during direct ozonation and O_3/H_2O_2 advanced oxidation process. Chemosphere 78 (5), 517–526. http://doi.org/10.1016/j.chemosphere.2009.11.037.

Qu, G., Lu, N., Li, J., Wu, Y., Li, G., Li, D., 2009. Simulataneous pentachlorophenol decomposition and granular activated carbon regeneration assisted by dielectric barrier discharge plasma. J. Hazard Mater. 172 (1), 472–478. http://doi.org/10.1016/j.jhazmat.2009.07.035.

Rezaei, F., Gorbanev, Y., Chys, M., Nikiforov, A., Van Hulle, S.W.H., Cos, P., Bogaerts, A., De Geyter, N., 2018. Investigation of plasma-induced chemistry in organic solutions for enhanced electrospun PLA nanofibers. Plasma Process. Polym. 15 (6), 1–18. http://doi.org/10.1002/ppap.201700226.

Sarangapani, C., Danaher, M., Tiwari, B., Lu, P., Bourke, P., Cullen, P.J., 2017. Efficacy and mechanistic insights into endocrine disruptor degradation using atmospheric air plasma. Chem. Eng. J. 326, 700–714. https://doi.org/10.1016/j.cej.2017.05.178.

Takamatsu, T., Uehara, K., Sasaki, Y., Miyahara, H., Matsumura, Y., Iwasawa, A., Ito, N., Azuma, T., Kohno, M., Okino, A., 2014. Investigation of reactive species using various gas plasmas. RSC Adv. 4 (75), 39901–39905. http://doi.org/10.1039/C4RA05936K.

Tang, S., Li, N., Qi, J., Yuan, D., Li, J., 2018. Degradation of phenol using a combination of granular activated carbon adsorption and bipolar pulse dielectric barrier discharge plasma regeneration. Plasma Sci. Technol. 20 (5), 054013. http://doi.org/10.1088/2058-6272/aaa7e9.

Tarabová, B., Lukes, P., Janda, M., Hensel, K., Sikurova, L., Machala, Z., 2018. Specificity of detection methods of nitrites and ozone in aqueous solutions activated by air plasma. Plasma Process. Polym. 15 (6), 1–12. http://doi.org/10.1002/ppap.201800030.

Vanraes, P., Wardenier, N., Surmont, P., Lynen, F., Nikiforov, A., Van Hulle, S.W.H., Leys, C., Bogaerts, A., 2018. Removal of alachlor, diuron and isoproturon in water in a falling film dielectric barrier discharge (DBD) reactor combined with adsorption on activated carbon textile: reaction mechanisms and oxidation by-products. J. Hazard Mater. 354, 180–190. http://doi.org/10.1016/j.jhazmat.2018.05.007.

Verlackt, C.C.W., Neyts, E.C., Bogaerts, A., 2017. Atomic scale behavior of oxygen-based radicals in water. J. Phys. D Appl. Phys. 50 (11), 11LT01. http://doi.org/10.1088/1361-6463/aa5c60.

Von Gunten, U., 2003. Ozonation of drinking water: part I. Oxidation kinetics and product formation. Water Res. 37 (7), 1443–1467. http://doi.org/10.1016/S0043-1354(02)00457-8.

Wang, H., Zhan, J., Yao, W., Wang, B., Deng, S., Huang, J., Yu, G., Wang, Y., 2018. Comparison of pharmaceutical abatement in various water matrices by conventional ozonation, peroxone (O_3/H_2O_2), and an electro-peroxone process. Water Res. 130, 127–138. https://doi.org/10.1016/j.watres.2017.11.054.

Wardenier, N., Vanraes, P., Nikiforov, A., Van Hulle, S.W.H., Leys, C., 2019. Removal of micropollutants from water in a continuous- flow electrical discharge reactor. J. Hazard Mater. 362, 238–245. http://doi.org/10.1016/j.jhazmat.2018.08.095.

Wols, B.A., Hofman-Caris, C.H.M., 2012. Review of photochemical reaction constants of organic micropollutants required for UV advanced oxidation processes in water. Water Res. 46 (9), 2815–2827. http://doi.org/10.1016/j.watres.2012.03.036.